Mechanics of Materials 153 (2021) 103668

Contents lists available at ScienceDirect

Mechanics of Materials

journal homepage: www.elsevier.com/locate/mechmat

Characterization of polypropylene (PP) and poly(ethylene terephthalate) (PET) multifilament braided textile structures for Achilles tendon partial substitution

D.S. Morais [a,b], J. Cruz [c], R. Fangueiro [c], M.A. Lopes [a,*], R.M. Guedes [b,d]

[a] LAQV – REQUIMTE, Departamento de Engenharia Metalúrgica e Materiais, Faculdade de Engenharia, Universidade do Porto, Rua Dr. Roberto Frias, 4200-465, Porto, Portugal
[b] INEGI-Instituto de Engenharia Mecânica e Gestão Industrial, Rua Dr. Roberto Frias, 4200-465, Porto, Portugal
[c] Centre for Textile Science and Technology, University of Minho, Portugal
[d] Departamento de Engenharia Mecânica Faculdade de Engenharia, Universidade do Porto, Rua Dr.Roberto Frias, 4200-465, Porto, Portugal

ARTICLE INFO

Keywords:
Polypropylene
PP
poly(ethylene terephthalate)
PET
Braided structure
Textile
Tendon

ABSTRACT

When tendon injuries present a too large damage extension, the conventional treatment options do not result, so a new prosthetic device needs to be developed to partially replace a tendon. Therefore, in this study, different braided textile structures based on polypropylene (PP) and poly (ethylene terephthalate) (PET) multifilament yarns were developed, using a textile technology-based technique, in order to mimic the fibrous structure of tendons. Structures with different architectures were developed using different PP or PET yarns number and different braiding take-up rates, which consequently leads to different braid angles. The braids architecture influenced the porosity level, swelling profile, wicking ability and mostly their mechanical behavior. It was observed that the load at failure of the braids was mainly controlled by the number of yarns, but the strain level was mostly influenced by the take-up rate and consequently by the braid angle. Regarding the stiffness level, it results from a combination of the yarns number and braid angle. The structure based on 16 PET yarns, produced with the highest take-up rate, revealed a very promising creep and force-relaxation behavior for the final application, as well as a very interesting fatigue resistance.

1. Introduction

Tendons are classified as dense regular connective tissues and they physically bind muscles to skeletal structures, allowing locomotion and joint stability. Nowadays, occupational but mainly sporting injuries of tendons, ranging from repetitive strain injuries to complete ruptures, are among the most common health problem affecting adult population. The number of overuse injuries in the USA, for instance, is estimated to be about 30%–50% of all sports-related injuries, besides 51% of people over 80 years experiencing rotator cuff injury and 11% of regular runners suffer from tendinopathy in Achilles tendon (AT) (Chen et al., 2009; Hess, 2010; Maffulli et al., 2005). In some cases, in which the extension of tendon damage is too large, the conventional treatment options, such as repair surgery or biografts, maybe not efficient to recover the tissue functionality. Therefore, to accomplish a treatment solution for extensive damage of the tissue, other scaffolds are being developed by researchers to be used as prosthetic devices to partially replace a tendon (Morais et al., 2015).

As a connective tissue, tendons and ligaments are composed of cells and mainly of extracellular matrix (ECM), which has high density of type I collagen fibers. The complex hierarchical fibrous structures of collagen are responsible for the very complex tissue mechanical properties. Tropocollagen molecules, which are the structural unit of type I collagen, are assembled into microfibrils, which then assemble to form fibrils, which finally assemble into a tendon fiber. These fibers are arranged in regular patterns, namely in parallel arrays (Maffulli et al., 2005; Kuo et al., 2010; Sharma and Maffulli, 2006). A typical stress-strain curve of these tissues presents an initial "toe region" (~2% strain), in which the tissue accommodates the applied load by straightening its crimp pattern, followed by a linear relationship between load and strain where tendons can be strained to about 4% and then plastically deformed with microscopic and macroscopic tearing.

* Corresponding author.
E-mail address: malopes@fe.up.pt (M.A. Lopes).

https://doi.org/10.1016/j.mechmat.2020.103668
Received 5 January 2020; Received in revised form 11 November 2020; Accepted 13 November 2020
Available online 19 November 2020

The mechanical properties, which depend on the thickness and collagen content of the tissues that vary with its function and with patient age and condition, in general, present average values of the tensile strength of 50–150 MPa, Young's Modulus in the range of 1–2 GPa, an average stiffness of 200 N/mm and ultimate strain values of 4–10% (Morais et al., 2015; Lim et al., 2019; Santos et al., 2017; Karathanasopoulos et al., 2019; Martin et al., 1998).

Therefore, when designing a scaffold for tendon substitution it must be taken into account this complex fibrous micro-architecture of the tissue and the consequent mechanical performance.

A simple tubular braid is a textile structure formed by crossing a number of yarns/strands diagonally in such a way that each group of yarns/strands pass alternately over and under a group of yarns/strands laid up in the opposite direction (Omeroglu, 2006; Rawal et al., 2015; Kyosev, 2014). Due to its structural integrity, durability, design flexibility and precision, braided structures have been used for different critical applications (Omeroglu, 2006; Kyosev, 2014). Regarding the braiding pattern, which consists of the intersection repeat of the yarn groups, these structures may be classified as diamond (1/1 repeat), regular (2/2 repeat), which is the most used, or Hercules (3/3 repeat). Besides that, the braided structures can even be categorized as biaxial or triaxial, according to the orientation of the constituent yarns/strands. In general, both types of braids have two sets of braider yarns/strands placed in the clockwise and counter-clockwise directions (typically each yarn/strand aligned in the bias direction), whereas triaxial braids also have an additional set of strands aligned in the direction of braid axis (Rawal et al., 2015; Kyosev, 2014; Schwartz, 2008). In general, the tensile properties of braided structures are strongly dependent on their architecture and the kinematics and mechanics involved in the braid formation (Omeroglu, 2006; Rawal et al., 2015).

As base materials for scaffolds for tendons repair substitution, different natural and synthetic polymers have been studied (Morais et al., 2015; Rodrigues et al., 2013). The natural polymers despite their potential for tissue-engineered approaches combining biological and engineering sciences to regenerate interfaces such as tendon-to-bone, usually fail when used in the scaffold itself due to their inappropriate mechanical performance (Morais et al., 2015; Longo et al., 2010; Calejo et al., 2019). Therefore, in this study different braided textile structures, based on polypropylene (PP) and poly (ethylene terephthalate) (PET) multifilament yarns, were produced using a textile technology-based technique. Those fibrous structures will afterward be associated and arranged to form a more complex structure and mimic the complex fibrous micro-architecture of tendons and consequently their mechanical behavior. The used synthetic fibers are among the most popular in textiles for different applications, since the 1950s, and they present an interesting force-strain curve shape for the purposed application (Hearle and Morton, 2008). Moreover, both polymers have been used in different medical devices, such as abdominal meshes biomaterials, presenting a good biocompatibility level (Saxena et al., 2011; Veleirinho et al., 2014).

2. Materials and methods

2.1. Textile structures production

PP and PET multifilament yarns, with a linear density of 1200 and 1112 dtex respectively, were purchased from *Sarla Europe, LDA* (Portugal) to produce different biaxial braided structures on a vertical braiding machine with 16 carriers, under controlled process conditions. These filaments were chosen after analysing the medical-grade filaments available in the market and therefore avoiding the indoor production in future industrial scale production. For each yarn type, four different braided structures were produced, using always the same pattern (1/1) but different yarns number (6, 8 and 16) and/or take-up rate (H and L), as presented in Table 1. The take-up rate was changed by using change gears and two different levels were used, the higher level (H) was of 3.94 cm/s and the lowest level (L) was of 1.44 cm/s.

2.2. Structural and physicochemical properties

Scanning electron microscopy (SEM) analysis was performed, using a *FEI Quanta* 400 FEG *ESEM* microscope, in order to analyze the surface morphology of PP and PET yarn filaments and estimate the diameter of the yarns. The SEM images were acquired using the secondary electrons mode and the filaments elemental composition was evaluated by energy-dispersive X-ray spectroscopy (EDS).

The X-ray diffraction (XRD) analysis of the PP and PET yarns was performed using a *Bruker AXS D8 Discover* diffractometer, in mode θ-2θ, using a step size of 0.04° and an integration time of 1 s. For the identification of each crystalline phase and estimation of the crystallinity percentage (%x_c), it was used the *EVA* software using the equation: , where A_c is the area of the crystalline phase and A_a is the area of the amorphous phase of the diffractograms.

The swelling profile of the PP and PET yarns was evaluated by immersion of the yarns in phosphate-buffered saline solution (PBS, pH 7.4), using 5 samples of each. Firstly, each sample was weighed before immersion (), about 0.1 g. Afterward, the samples were placed in a mesh and immersed in the PBS solution and incubated at 37 °C, for 15 or 30 min. The mesh was then removed, the excess solution was removed by absorbent paper, during which the samples were shaken and then left 5 min air drying before weighting () the PP or PET yarn. The weight change () of each sample represents the water absorption and was calculated using the equation: . The vertical wicking ability of the PP and PET yarns and braided structures was evaluated, according to *Fangueiro R.* et al., using 5 samples of each polymer of 20 cm length, which were suspended vertically with its bottom end dipped in a reservoir of distilled water with a color agent (Fangueiro et al., 2010). The bottom end of each specimen was clamped with a clip to ensure that it could be immersed vertically at a depth of 3 cm into the colored water. The wicking heights, measured every minute over 10 min, were recorded.

All the textile structures were observed under no loading applied in triplicate by optical microscopy in order to estimate their diameter and their braid angle through the treatment of the images by the software *J*

Table 1
Production parameters and textile properties of the produced structures, using PP or PET multifilament yarns.

Polymeric material	Textile structure	Number of filaments (yarn)/yarns (braid)	Take-up rate (cm/s)	Braids/cm	Linear density (tex)	Tenacity (N/tex)
PP	**Yarn**	137 ± 4	–	–	120	0.62 ± 0,06
	6 YH	6	H	–	679 ± 5	0.60 ± 0,02
	8 YH	8	H	1.2 ± 0.1	1103 ± 4	0.51 ± 0,01
	8 YL	8	L	3.2 ± 0.2	1183 ± 5	0.48 ± 0,04
	16 YH	16	H	2.2 ± 0.1	1862 ± 6	0.58 ± 0,03
PET	**Yarn**	162 ± 4	–	–	111	0.66 ± 0,07
	6 YH	6	H	–	682 ± 3	0.56 ± 0,04
	8 YH	8	H	1.4 ± 0.1	903 ± 5	0.65 ± 0,03
	8 YL	8	L	3.5 ± 0.2	943 ± 7	0.59 ± 0,07
	16 YH	16	H	2.4 ± 0.1	1835 ± 5	0.64 ± 0,07

image. In order to assess the total porosity volume of each textile structure, 3 samples with 20 cm length were cut and the geometrical volume () was calculated considering each sample as a cylinder. Each sample was weighted () to determine the theoretical volume (if the cylinder was composed of 100% of PP or PET (). Thus, the porosity percentage () can be calculated in accordance with the equation: .

2.3. Mechanical properties

The yarn-on-yarn abrasion was evaluated, according to CY 1503–00 from Cordage Institute International Standard (Cordage Institute Interna, 2001), in a system where two portions of one yarn are inter-twisted (3 intertwisting wraps), they rub against one another under controlled tension due to the cyclic motion (72 rpm) imposed by rotation of a crank to which the yarn is attached. The tension is imposed by a weight of 2% of the yarn tensile maximum force and the number of cycles until the yarn failure was recorded for 5 samples.

2.3.1. Static mechanical behavior

The tensile properties of the yarns and braids were evaluated by performing uniaxial tensile tests (5 samples of each) on *Lloyd instruments LR 30K* equipment, in displacement control, up to rupture. The initial distance between grips was defined as 235 mm and the displacement rate as 8.5 mm/s in order to compare the experimental results with some reported data of native tissues. Mechanical properties such as stiffness (N/mm), load at failure (N) and strain to failure (ε, %) of all structures were measured. It should be observed no significant pre-tension was applied. Although no specific standard was followed, the procedures adopted the recommendations of CY 1503–00 from Cordage Institute International Standard (Calejo et al., 2019). A full-scale mechanical test of the device was done to circumvent any scale effects due to the intrinsic complexity of the fibrous structure. Assuming a total Achilles tendon replacement, the distance between grips, i.e. 235 mm, represents an average length of the achilles tendon (Intziegianni et al., 2015). The deformation rate imposed was 3.6%/s, which is slightly above the typical quasi-static strain rate, i.e. 1%/s (Wren et al., 2001). Mechanical properties of the human achilles tendon. Clinical Biomechanics, 16 (3), 245–251]. This is lower than the strain rate experienced during running, i.e. around 16%/s, assuming a frequency of 1.37 Hz and maximum strain levels of 6% during each stride (Lichtwark et al., 2013) and 10%/s for (Wren et al., 2001).

The tensile properties of the PP and PET yarns were also evaluated after possible degradation by hydrolysis. For that, yarn samples were immersed in 4 mL of PBS (pH 7.4) (5 samples of each) and their initial weight was previously recorded. All samples were incubated at 37 °C and under 60 rpm agitation. After 15 days, 1, 2, 4, 8, 12 and 18 months, the PP and PET yarn samples were removed, dried at room temperature, weighed and subjected to a tensile test with the parameters indicated before.

2.3.2. Time-dependent mechanical behavior

2.3.2.1. Creep and relaxation tests. In creep tests, PET 16 YH braid samples were uniaxially loaded to 30, 50 or 70% of their load at failure in 20 s and kept at this level for about 1000 s. After this holding phase, they were ramped down reaching the 0 N force after another 1000 s. In case of relaxation tests, PET 16 YH braid samples were stretched to 30, 50 or 70% of their strain to failure at failure in 20 s and then kept at this level for about 1000 s. After this holding phase, they were ramped down reaching the 0% strain after another 1000 s. Both tests were performed in triplicate for each percentage on *Instron ElectroPuls E1000* equipment with a load cell of 2 kN and the initial distance between grips was defined as 235 mm.

Residual, unrecovered or permanent strain is a critical aspect of the viscoelastic/viscoplastic response of polymers. This conducted to the need of dividing the tests into the three stages, mentioned before, 1) loading, 2) constant load or strain during 1000s and 3) unloading for another 1000s. By establishing an unloading stage, after creep loading, the protocol allows a measure of the amount of recovered strain during a certain period, in the present case 1000s. Therefore, the strain measured at 1000s is expected to be proportional to the permanent strain. This allows a coherent comparison of permanent strain for different load levels using short-term creep mechanical tests.

2.3.2.2. Monotonic cyclic tests. In fatigue tests, PET 16 YH braid samples, constantly being hydrated with PBS (pH 7.4), were exposed to a sinusoidal load until failure or in limit up to 1 million cycles. The applied sinusoidal load, at a frequency of 5 Hz, was defined using a maximum load corresponding to 30, 50, 65 or 70% of their load at failure and a minimum load corresponding to 10% of the load at failure being used. The tests were performed in triplicate for each percentage on *Instron ElectroPuls E1000* equipment with a load cell of 2 kN and the initial distance between grips was defined as 235 mm.

2.4. Statistical analysis

Experimental data is presented as mean ± SD (standard deviation). Statistical analysis of data was performed using the one-way ANOVA test with Bonferroni post hoc analysis, using the software SigmaStat 3.5. The differences were considered to be significant at a level of $p < 0.05$.

3. Results

3.1. Structural and physicochemical properties

3.1.1. SEM analysis

In Fig. 1A/1. B and 1. C/1. D, it is possible to observe, by SEM analysis at two different magnifications (140× and 2500x), that the PP and PET yarns are composed by several filaments, which are all aligned in parallel. In Fig. 1B and 1. D, it is possible to observe the surface morphology of the PP and PET filaments, which is smooth and homogeneous, being detectable only some punctual defects. Besides that, as expected, the acquired EDS spectra revealed the high level of C content in PP filaments and in case of PET filaments the presence of C and O (data not showed). Based on SEM images the diameter of the yarns was also estimated, being about 989.0 ± 1.7 μm in case of PPP and about 830.8 ± 1.6 μm in case of PET.

3.1.2. XRD analysis

In Fig. 2A, it is presented the XRD spectrum of the PP yarn, which presents peaks at positions 2θ of about 14°, 17°, 18.5°, and 21.8°. The crystallinity percentage ($\%x_c$) for the PP yarns according to the XRD data was estimated as about 61.2% ± 1.1.

In Fig. 2B it is presented the XRD spectrum of the PET yarn, which presents peaks at positions 2θ of about 17.6°, 22.8°, and 25.6°. The $\%x_c$ for the PET yarns according to the XRD data was estimated as about 55.0% ± 3.2.

3.1.3. Yarns swelling profile

Fig. 3A and 3. B show the weight change of the PP and PET yarn respectively, after immersion in water over 30 min. As observed, after the first 15 min there is an increase in the yarn weight of about 270% in the case of PP and about 135% in case of PET. After 30 min of immersion there is no significant change in weight for both yarns.

3.1.4. Optical microscopy

Fig. 4 presents the optical microscopic images of all braided structures based on PP (Fig. 4A, 4B, 4C and 4D) or PET yarns (Fig. 4E, 4F, 4G and 4H), which may be classified as biaxial attending to the orientation of the constituent yarns and as diamond, in case of braids with 6 and 8

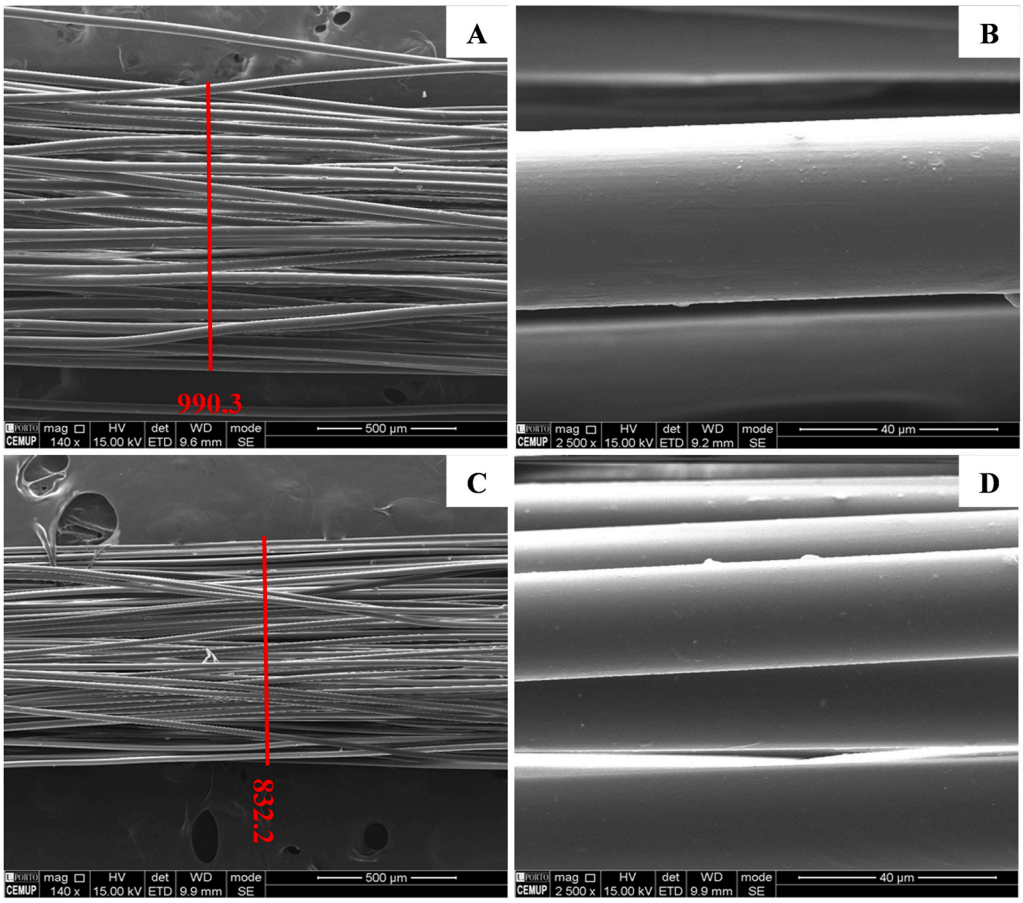

Fig. 1. SEM images of the PP multifilament yarn: (**A**) 140x and (**B**) 2500x; and of the PET multifilament yarn: (**C**) 140x and (**D**) 2500x.

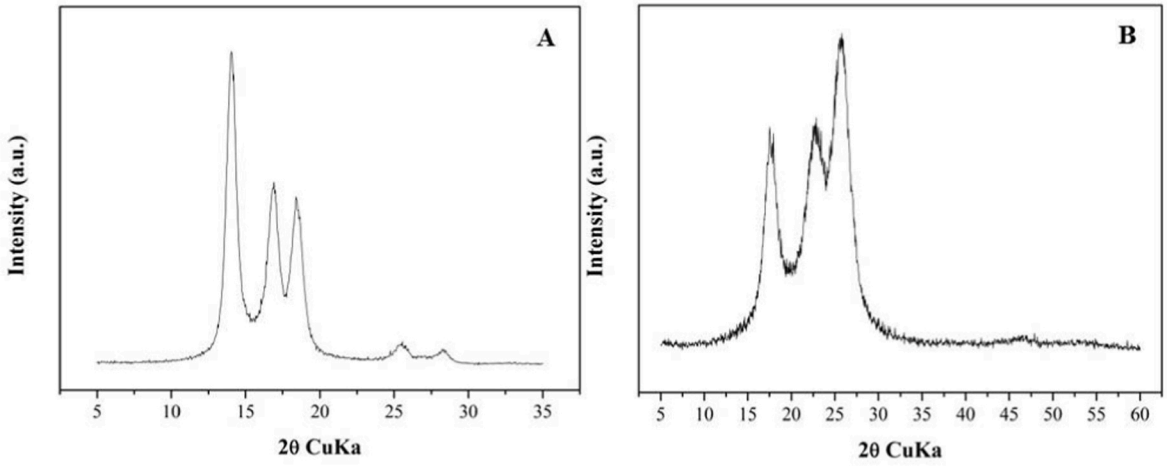

Fig. 2. X-ray diffractograms of the PP (**A**) and PET (**B**) multifilament yarns.

yarns, and as regular, when using 16 yarns, attending to the braiding pattern. In this Fig. 3, it is possible observe the braids architecture and how the multifilament yarns are arranged among them. Using these images the braids diameter, presented in Fig. 3, and braids/cm, presented in Table 1, was estimated. As presented, for the same yarn and take-up rate, both parameters tend to increase as the number of yarns in the structure increases. Besides that, comparing the same braided structure but with different yarn types, the diameter is higher when using the PP yarn. Regarding the braids/cm, when using the same yarns number, it is higher when the take-up rate is lower.

Moreover, also based on optical microscopic images, the braid angle was calculated, which represents the acute angle that each yarn makes with the braid longitudinal line, as marked with red lines. As observed in Fig. 5, for the same take-up rate, as the number of yarns increases the braid angle also increase using any one of the yarns, however for the same structure the braid angle is higher when using the PP yarn. In the case of PP (Fig. 5A), when the number of the yarns increases from 6 to 16 the angle rises from about 6.9° ± 0.4 to 16° ± 1.6. In case of PET (Fig. 5B), when the yarns number increases from 6 to 16 the angle rises from about 4.6° ± 0.4 to 13.4° ± 0.9. When using 8 yarns of any one of

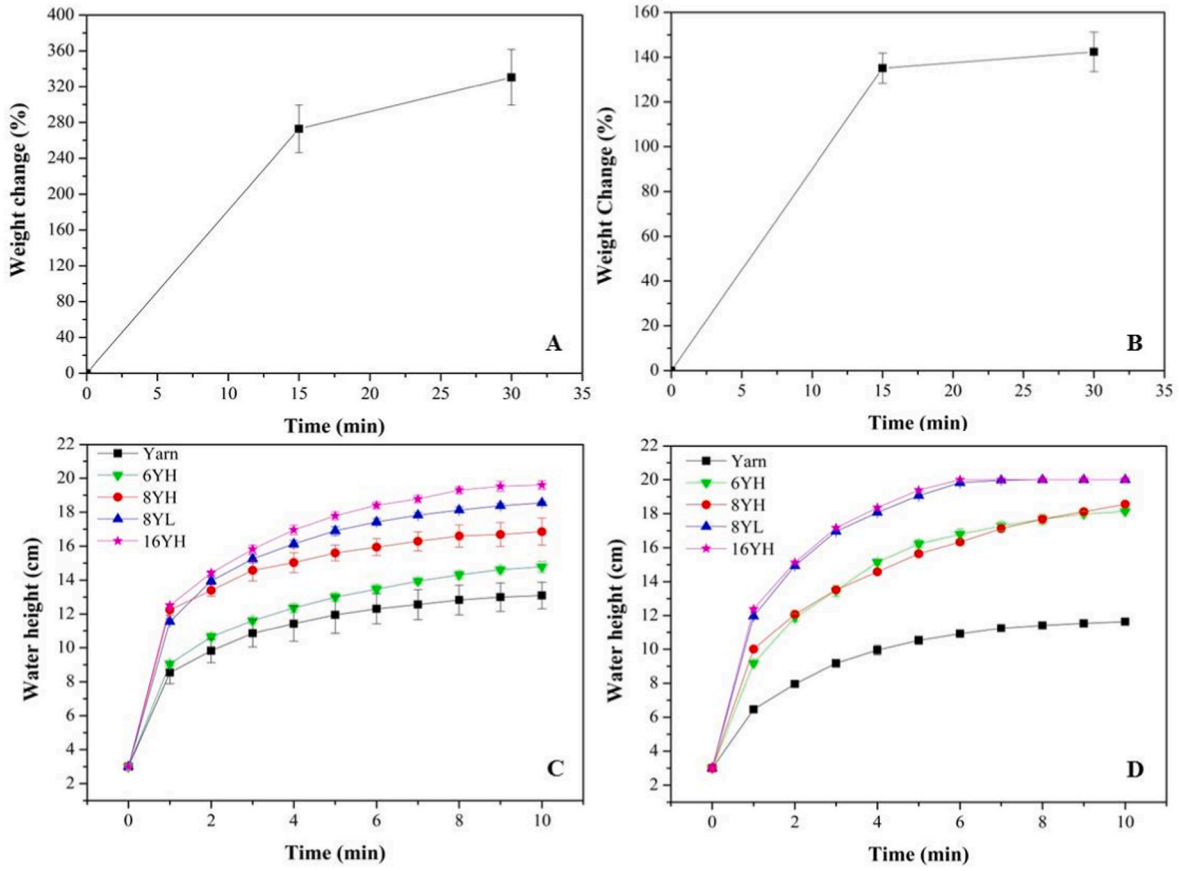

Fig. 3. Weight change of the PP yarn (A) and PET yarn (B) over the immersion time in PBS. PBS solution height along the PP yarn or the braided structures (C) and PET yarn or the braided structures (D) over 10 min. Data are presented as mean ± SD.

the materials, the braid angle is significantly higher when the take-up rate is lower (8 YL).

3.1.5. *Braids porosity*

In Fig. 6 is presented the porosity level of each braided structure using the PP (Fig. 6A) or PET yarns (Fig. 6B). As observed, for both yarns, the porosity level does not present a significant change as the number of yarns or take-up rate changes. Even so, using each one of the yarns, the highest porosity level is observed for the 16 YH structure, which is about 88% in the case of PP and 85% in case of PET.

3.1.6. *Wicking profile*

In order to evaluate the yarns and braids wicking profile, in Fig. 3C and 3. D is presented the water height level along the yarns or braids, which increases over time for all PP and PET-based textile structures. In case of PP, at the first minute, the yarn and the 6 YH braid present a water height of about 8 cm, which is lower than the height in case of 8 YH, 8 YL and 16 YH braids, which present a similar value of about 12 cm. Until about 4 min, the yarn and the 6 YH braid present always a very similar height and the other 3 braids present similar values among them. However, after those 4 min the water height becomes significantly different among the yarn and all braids, being observed the highest water height for the 16 YH braid, then for 8 YL, 8 YH, 6 YH and finally for the yarn. Regarding the PET structures, at the first minute, the yarn presents the lowest water height of about 6 cm, then the 6 YH and 8 YH braids present a value of about 10 cm and the highest value of about 12 cm is observed for 8 YL and 16 YH. After the first minute, over time, the water height relation among the yarn and braids remains the same, the yarn presents always the lowest value, the 6 YH and 8 YL present a middle value and the 8 YL and 16 YH present the highest height value.

3.2. *Mechanical properties*

Regarding the abrasion resistance of the used multifilament yarns, PP yarns were able to withstand about 959 ± 160 cycles and PET yarns a much greater number of cycles, namely about 14742 ± 1142.

3.2.1. *Static mechanical behavior*

Fig. 7. A represents the force-strain curves of tensile tests of the PP yarn and braids, where is possible to observe that all braids present curves with a similar shape. However, they present different values of load at failure, as observed in Fig. 7C, and strain to failure, as observed in Fig. 7D. The yarn presents the lowest force at failure and regarding the braids, for the same take-up rate, the force increases as the number of yarns in braid increases (6 YH, 8 YH, and 16 YH). Comparing the braids with the same number of yarns with different take-up rates (8 YH and 8 YL), the load at failure is very similar between them. Regarding the strain at failure, when the yarns number increases for the same take-up rate there is no significant difference among the braids. However, between 8 YH and 8 YL there is a significant difference in strain to failure, being higher in case of 8 YL. Moreover, in Fig. 7B it is possible to observe the stiffness difference among the braids, which increases when the number of yarns increases, but decreases when the take-up rate is lower for the same yarns number.

Regarding PET braids, the force-strain curves are presented in Fig. 8A. It is possible to observe that all braids present curves with a similar shape, but with different values of load at failure, as observed in Fig. 8C, and strain to failure, as observed in Fig. 8D. The yarn presents the lowest force at failure and regarding the braids, for the same take-up rate, the load at failure increases as the number of yarns in braid increases (6 YH, 8 YH and 16 YH). Comparing the braids with the same

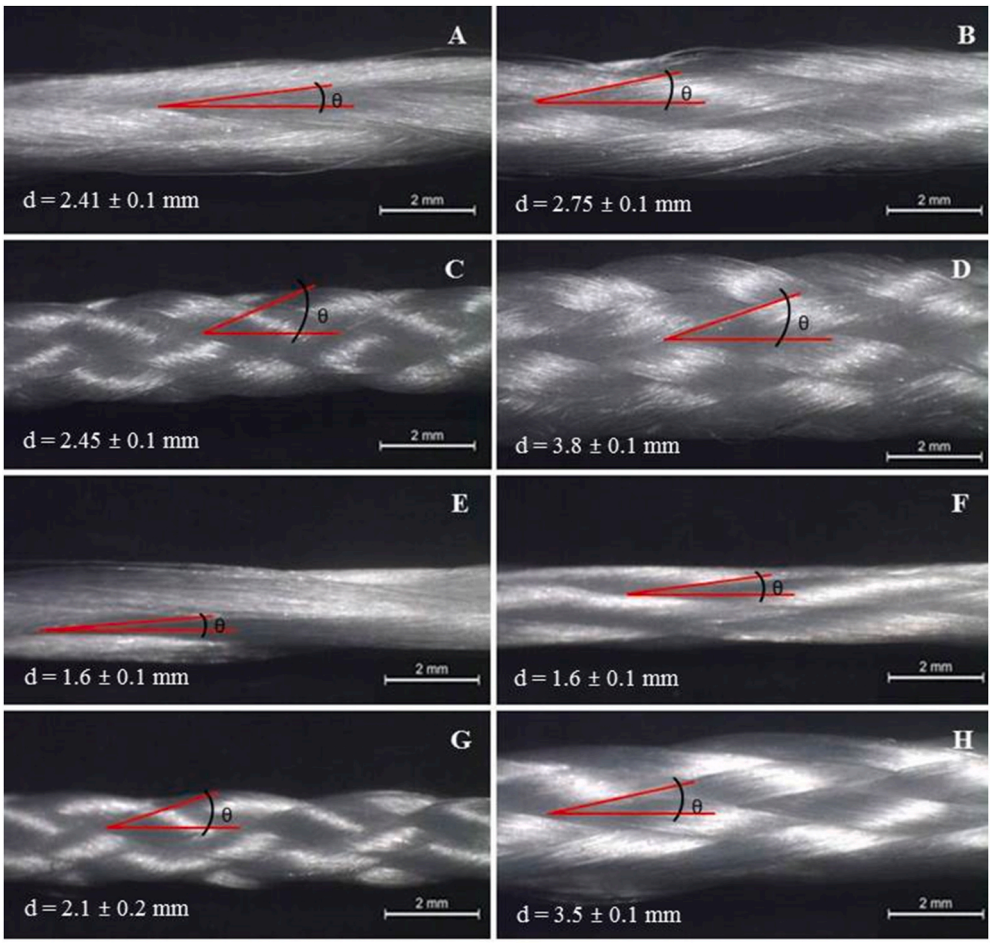

Fig. 4. Optical microscopic images of PP braided structures: (**A**) 6 YH; (**B**) 8 YH; (**C**) 8 YL; (**D**) 16 YH. Optical microscopic images of PET braided structures: (**E**) 6 YH; (**F**) 8 YH; (**G**) 8 YL; (**H**) 16 YH.

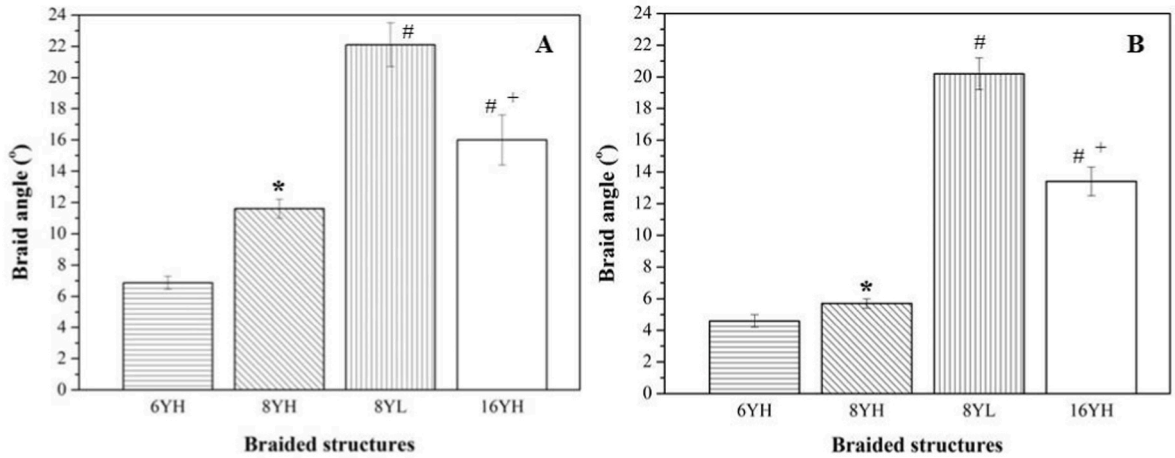

Fig. 5. Braid angle of the textile structures based on PP yarns (**A**) and PET yarns (**B**). Data are presented as mean ± SD. $p < 0.05$-significant difference compared to 6 YH (*), 8 YH (#) and 8 YL (+).

number of yarns but with different take-up rates (8 YH and 8 YL), the load at failure is very similar between them. Regarding the strain at failure, when the number of the yarns is the same but using a different take-up rate, there is no significant difference among the braids. Moreover, in Fig. 8B it is possible to observe the stiffness difference among the braids, which increases with the number of yarns and the take-up rate.

It should also be referred that after immersion in PBS, for degradation evaluation, the yarns samples do not reveal significant weight change and their tensile properties remained constant (data not shown).

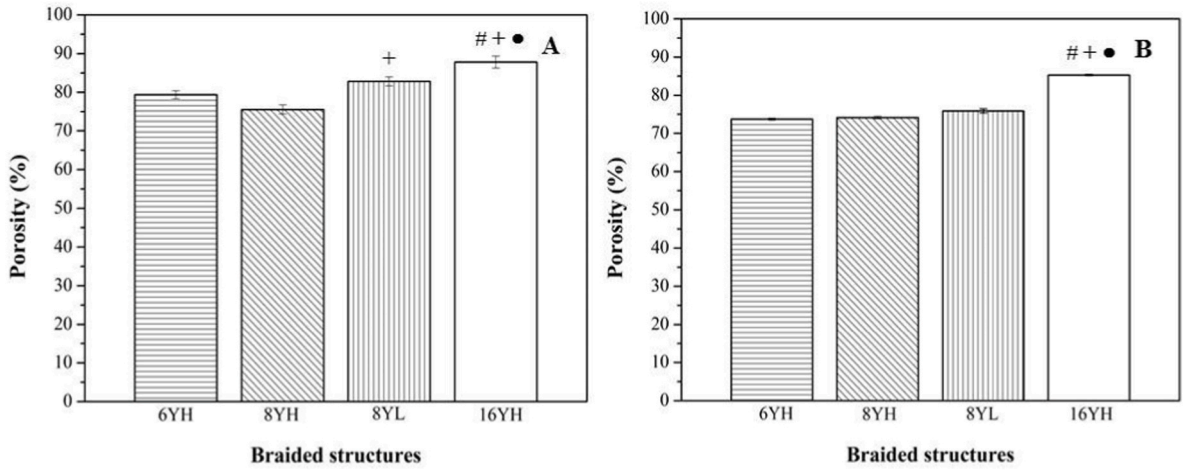

Fig. 6. Porosity (%) of the textile structures based on PP yarns (**A**) and PET yarns (**B**). Data are presented as mean ± SD. $p < 0.05$-significant difference compared to 6 YH (#), 8 YH (+) and 8 YL (•).

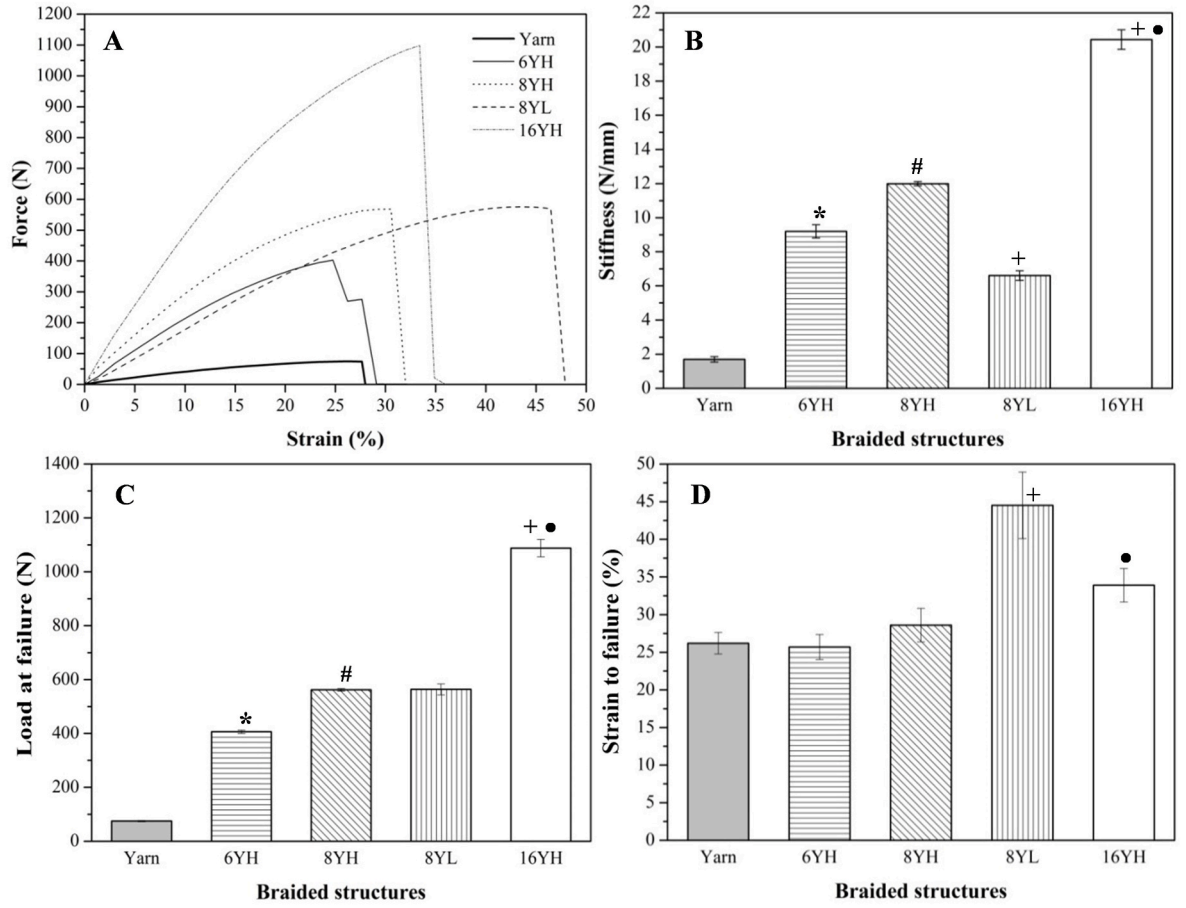

Fig. 7. (**A**) Force-strain curves of the PP yarn and all braided structures. Tensile properties of the PP yarn and all braided structures: (**B**) stiffness, (**C**) load at failure and (**D**) strain to failure. Data are presented as mean ± SD. $p < 0.05$-significant difference compared to yarn (*), 6 YH (#), 8 YH (+) and 8 YL (•).

3.2.2. *Time-dependent mechanical behavior*

3.2.2.1. Creep and relaxation tests. Fig. 9A and 9. C show the results of creep and relaxation behavior of the 16 YH structure composed by PET yarns. As observed in Fig. 9A, as higher is the applied force on the structure higher is the reached strain level, which slightly increases over the 1000 s of loading. This behavior is evident when plotting the most linear region of the different creep curves in a Log-Log scale, where is possible to observe the very low and similar creep rate for all force levels. The values of the permanent strain (ε_p), which is very similar for all force levels, and the recoverable strain (ε_r), which increases when the force level increases, are presented in Table 2.

Regarding the relaxation behavior, as observed in Fig. 9C, as higher is the applied force on the structure higher is the reached load level, which slightly decreases over the 1000 s. This behavior is evident when plotting the most linear region of the different creep curves in a Log-Log

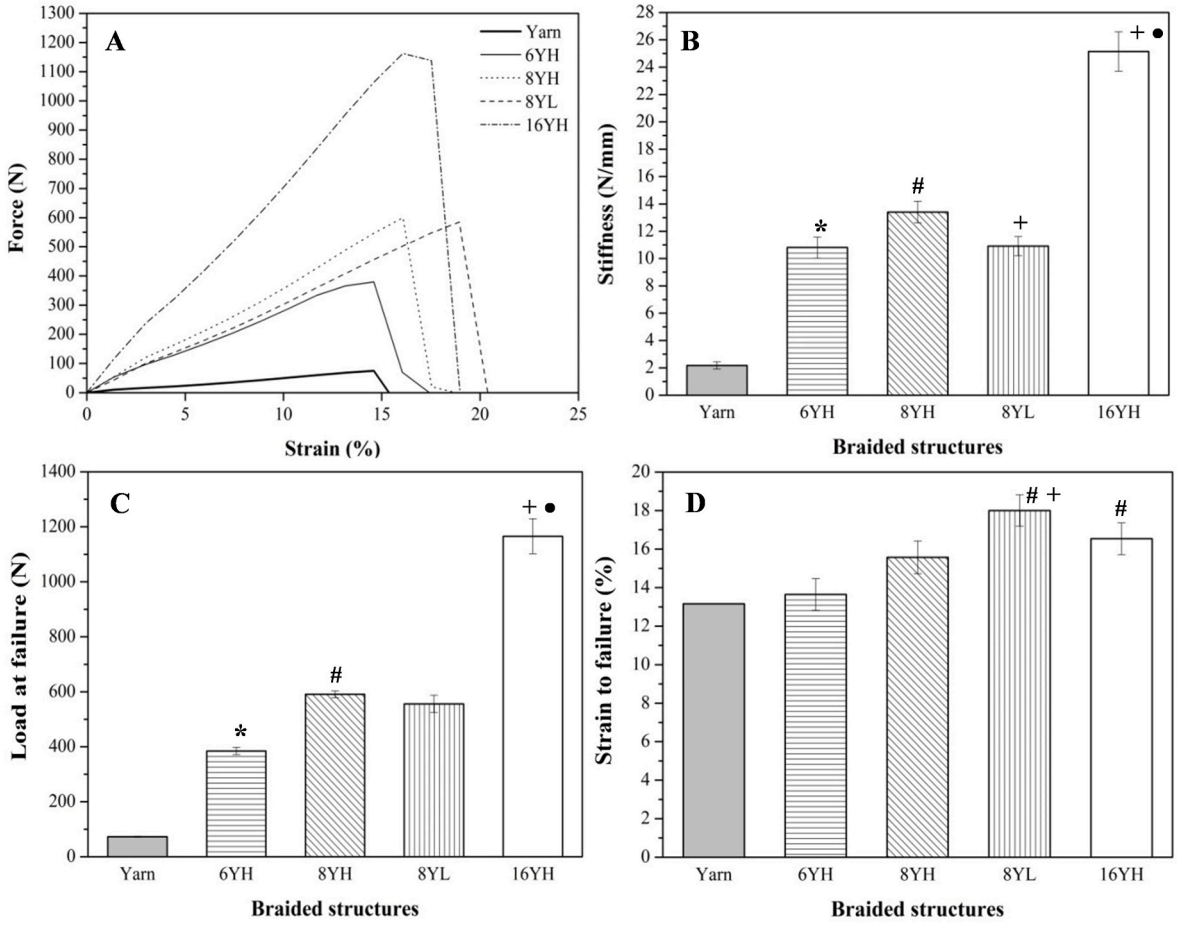

Fig. 8. (**A**) Force-strain curves of the PET yarn and all braided structures. Tensile properties of the PET yarn and all braided structures: (**B**) stiffness, (**C**) load at failure and (**D**) strain to failure. Data are presented as mean ± SD. $p < 0.05$-significant difference compared to yarn (*), 6 YH (#), 8 YH (+) and 8 YL (•).

scale, where is possible to observe the low and similar relaxation rate for all strain levels.

3.2.2.2. Monotonic cyclic test. The fatigue behavior of the PET-based 16 YH braid is presented in Fig. 10, where is possible to observe that as the load level increases the number of cycles that the structure is able to withstand decreases and a linear relation on the semi-logarithmic scale exists between the applied forces and the number of cycles to failure.

4. Discussion

The textile structures under study were designed based on multifilaments due to their higher permeability, swelling and wicking ability, and surface area than monofilament yarns, which are important features in a tissue regeneration process, as will be discussed in this section (Alagirusamy and Das, 2010; Potic et al., 2011). Moreover, the multifilament yarns may present a lower failure probability due to the phenomenon of size effect on the structural strength. In a monofilament yarn, when the load reaches a certain level, the break initiates from a flaw, which propagates across the fiber and it opens, owing to the drawing (high plastic extension) of the fiber remainder, until a final multiple crack zone completes the yarn failure. In a multifilament yarn, when the load reaches a certain level, smaller defects appear on their several tiny filaments, which propagate in a controlled manner. Even if some yarns filaments disrupt, other ones may keep the yarn cohesion and still withstand some loading (Hearle and Morton, 2008; Bažant, 1999; Vořechovský and Chudoba, 2006). Therefore, among different synthetic multifilament yarns, after tensile testing them and attending to the tenacity and stiffness levels, two multifilament yarns based on PET and PP, which have been used in several biomedical applications as biocompatible materials (Saxena et al., 2011; Modjarrad and Ebnesajjad, 2013; Ratner et al., 2004), were selected.

First of all, SEM analysis showed the smooth and homogeneous surface of the filaments of the yarns and that they are all aligned in parallel, what grants to the yarn a stiffness higher than if the filaments were not so well organized and longitudinally parallel. This alignment of all filaments with the loading axis, when the yarn is loaded in its longitudinal direction, leads to a higher stiffness. Moreover, the SEM images were also used to measure the diameter of the yarns, being the average presented in Fig. 1. As described in Table 1 the PP yarn, which has a linear density of about 1200 dtex, presents a diameter higher than PET yarn (about 989.0 against 830.8 μm), but the number of filaments is lower than in case of PET yarn (about 137 against 162 filaments). Thus, the PET filaments must be finer than PP filaments, as is possible to check on Fig. 1B and 1. D.

The XRD analysis was performed to evaluate the yarns' crystallinity level because it will influence their mechanical performance and biodegradability (Sarasua et al., 2011). The analysis indicated that both polymeric yarns are semi-crystalline. In case of PP yarn, its XRD spectrum shows characteristic peaks at positions 2θ of about 14°, 17° and 18.5°, which present a correlation with the ICDD sheet of PP (ICDD # 00-054-1936). However, another peak at 21.8°, which corresponds to the plan (140) and should have the second-highest intensity, should also be observed. The lack of this plane may be due to the preferential filaments orientation in the plan (110), which may have occurred during the yarns processing (Favaro et al., 2009). The XRD pattern of the PET

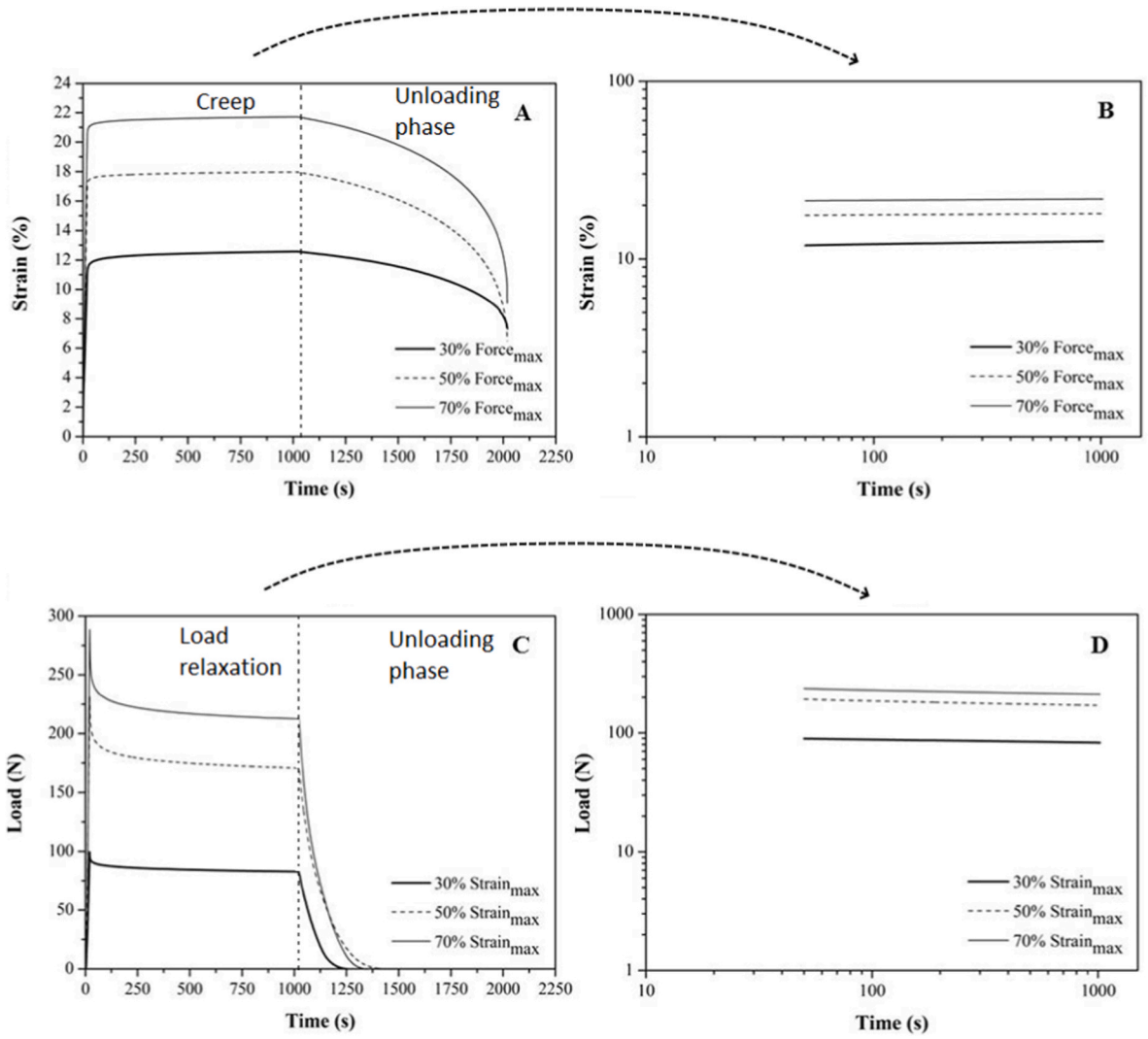

Fig. 9. Representative curves of creep behavior of PET-based 16 YH at different levels of force (**A**), in Log–Log scale (**B**). Representative curves of relaxation behavior of PET-based 16 YH at different levels of strain (**C**), in Log–Log scale (**D**).

Table 2
Permanent strain (ε_p) and recoverable strain (ε_r) for each creep level.

	Creep level (%)		
Strain (%)	30	50	70
$\varepsilon_p = \varepsilon_t \approx 2000$ s	10.6 ± 1.5	13.5 ± 0.8	11.0 ± 1.5
$\varepsilon_{max} = \varepsilon_t \approx 1000$ s	14.4 ± 2.3	19.4 ± 0.7	21.6 ± 0.6
$\varepsilon_r = \varepsilon_{max} - \varepsilon_p$	3.8 ± 1.2	6.5 ± 0.4	9.6 ± 0.7

yarn shows characteristic reflections of crystallinity relative to planes (010), (110) and (1000), for scattering angles 2θ of about 17.6°, 22.8° and 25.6°, respectively (Huang et al., 2012; Nunes et al., 2009). The crystallinity level for the PP and PET yarns, according to the XRD data, was estimated as 61.2% ± 1.1 and 55.0% ± 3.2 respectively (Balani et al., 2015). The amorphous regions in the filaments matrix act like a rubber to give extensibility to them, while the crystallites hold the structure together and limit the extensibility. When the degree of molecular orientation (crystallinity) increases, the strength of the filaments also increases, but there is a limit to how much draw can be applied without breaking the filaments (Hearle and Morton, 2008; Balani et al., 2015). So, the yarns crystallinity level will influence the stiffness (N/mm) of the yarns, i.e. the load level necessary to extend the yarn 1 mm.

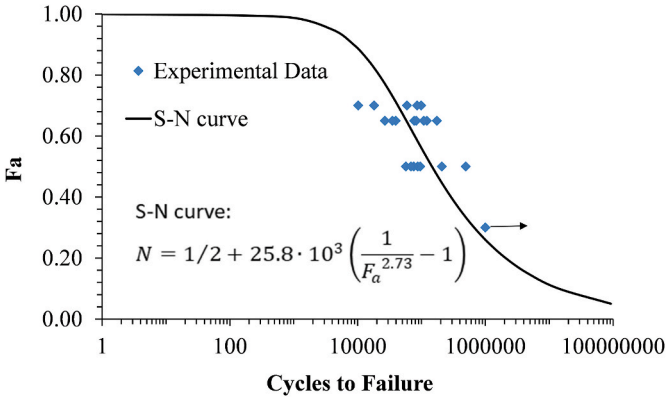

Fig. 10. Fatigue behavior of PET-based 16 YH braid**:** normalized applied force (Fa = Applied Load/Failure Load) vs cycles to failure (Note: All the specimens fatigued at 30% of the load at failure survived after 1 million cycles, noting the tests stopped after 1 million cycles).

For each one of the yarns, 4 different braided structures were produced, as presented in Table 1 and observed in Fig. 4. In general, for both yarns, for the same take-up rate (H), there is a trend, when the yarns

number increases the number of braids/cm tends to increase, as well as the diameter and linear density of the structure. The increase in diameter is easy to understand due to the increase of the cross-sectional area and the linear density increase was already expected due to the presence of more polymeric matter per structure length unity. Regarding the number of braids/cm, it is influenced by the number of yarns due to their different arrangements in braiding process. In case of using the same number of yarns but different take-up rates (8 YH and 8 YL), the number of braids/cm is higher for 8 YL, as presented in Table 1, because the number of braiding points/s is higher when the braiding take-up rate is lower. In spite of having the same number of yarns, the 8 YL structures diameter is higher than in the case of 8 YH structures due to the different yarns arrangement and compaction caused by the different number of braiding points. As consequence, the linear density is higher in case of 8 YL braid than in case of 8 YH, due to the higher number of braids/cm, meaning more polymeric material/cm.

During the braiding process, the yarns interlace diagonally, meaning that each yarn makes an angle with the structure longitudinal axis, as assigned in Fig. 4 with red lines, which can be between 1° and 89° but is usually in the range of 30°–80°. This angle is called the braid angle and is the most important geometrical parameter of braided structures (Omeroglu, 2006; Kyosev, 2014). As observed in Fig. 5, the braid angle increases when the number of yarns increases or when the take-up rate decreases. The braid angle of a structure is, of course, related to the number of braiding points/cm. Therefore, as already discussed, when the yarns number increases or the take-up rate decreases, the number of braids/cm tends to increase leading to a higher braid angle. These results are in accordance with literature that describes the same effect of the take-up rate and number of yarns on the braid angle (Omeroglu, 2006; Kyosev, 2014; Bicking and Oxenham, 2012) Besides that, comparing the same braided structure but with a different yarn type, PP_16 YH and PET_16 YH, the diameter and braid angle is slightly higher when using the PP yarn than the PET yarn, but the number of braids/cm tends to be higher when using the PET yarn. This may be related to the PP yarn higher diameter and its flattening/enlargement in the structure.

The porosity of a scaffold for living tissue regeneration can modulate the functionality and cellular response to the implant. Pore interconnectivity extending through an implant increases the overall surface area for cell attachment, enhancing its regenerative properties by allowing the tissue ingrowth into the structure matrix (Cooper et al., 2005; Laurencin and Freeman, 2005). Therefore, the porosity level of all produced structures was evaluated and it increased when the number of yarns increased to 16, which is about 88% in the case of PP and 85% in the case of PET. The porosity of the textile structures is mainly due to the open spaces among the yarns, but also due to smaller spaces among filaments composing each yarn, so when increasing the number of yarns it would be expected to have more open spaces. However, when increasing the number of yarns and keeping all other braiding parameters, the compaction among them is different, what is proved by the very similar diameter when using 6 or 8 yarns.

One of the scaffold's limitations is the ability to promote cell infiltration, oxygen and nutrients diffusion which is important to ensure cell attachment, proliferation, and differentiation. The scaffold design is a way to overcome these limitations and it has been proved that a high wicking ability increases fluid intake and enhances cell infiltration and distribution (Tabbaa and Burg, 2015; Oh et al., 2014; Tabbaa et al. Burg). In textile structures, the liquid transfer mechanisms include water diffusion and capillary wicking, which are mainly determined by effective capillary pore distribution, pathways and surface tension. Wicking is the spontaneous flow of a liquid in a porous substance, driven by the capillary forces. The flow and retention of water will be affected by the form and alignment of the open spaces in the structure, which depend on how the fibers are packed together. As capillary forces are caused by wetting, wicking is a result of spontaneous wetting in a capillary system. Besides that, wetting may cause the fabric swelling depending on yarns type, changing the capillary space position (Hearle and Morton, 2008; Fangueiro et al., 2010; Benltoufa et al., 2012). Therefore, in order to understand and evaluate this functionality, the swelling profile of the used yarns and wicking behavior of the yarns and braids were evaluated.

The water uptake (swelling) by the yarns occurs as a result of water entering into yarn structure once that the osmotic pressure is greater than the forces of the crosslinking bonds that maintain the structure of the polymeric structure. Water molecules diffuse into the amorphous regions of the yarn and break intermolecular hydrogen bonds, allowing an increase in the intermolecular distance of the polymer chains, which causes swelling. As a result, swelling increases the amorphous regions of the yarn (Akinli-Kogak, 2001; Adanur, 1995; Morais et al., 2013). Since the PP and PET yarns weight significantly increased after 15 min immersed in water, as observed in Fig. 3A and 3. B, it means that yarns swelling occurred due to the water absorption into the structure. However, after the 15 min until the 30 min, the swelling rate significantly decreased, indicating a saturation state. When swelling increases over time it means that the intermolecular spaces of the yarns are still being filled with water until it reaches a saturation point, where an equilibrium state with aqueous medium is reached, meaning that the osmotic pressure is balanced in and out of the structure by the forces of the crosslinking bonds (Akinli-Kogak, 2001; Morais et al., 2013; De et al., 2002). In addition, it must be noticed that the swelling level for the PP yarn is always higher than for PET yarn, what may be explained by the lower water contact angle in case of PP than in case of PET, allowing an easier water entrance.

Capillary rise within a textile is influenced by the structure architecture, namely by its porosity, yarns content and braid angle, which will influence the inter- and intra-yarns pores dimension and distribution (pathways) along the structure and consequently the quality of the capillary channels. A structure with more capillary spaces will have a high capillary rise. In Fig. 3C and 3. D, it is possible to observe that as the number of yarns increases, for the same take-up rate, the water height at each time point also increases. When comparing the 4 braids with the respective yarn, the significant higher water height is explained by the significant increase of inter- and intra-yarns pores. Comparing the 16 YH with all other structures, this phenomenon could also be explained by the amount of inter- and intra-yarns pores, which is slightly higher than in other braids (Fig. 6). However, as already discussed, for both materials types, when the number of yarns changes from 6 to 8 there is no difference in porosity level. So, when using PP yarns, the wicking difference between these two structures may be due to the different pores distribution. Regarding the structures produced with 8 yarns, the 8 YH presented a lower capillary rise than the 8 YL. However, once since 8 YH and 8 YL present a porosity level very similar, it means the braiding angle and consequently the braid architecture may have a high importance on the capillarity. The different architecture may create pores with different sizes and distribution, creating capillary channels with a lower or higher capillary pressure (Oh et al., 2014). Moreover, with increasing time, namely after about 6 min, the water height tends to stabilize, which may be explained by the saturation state already discussed. During the diffusion of the liquid into the yarn the capillary action and diffusion mechanisms are coupled, and the swelling generally reduces the dimensions of the yarn pore space, decreasing the rate of absorption over time. In an extreme case, some kind of *blocking* occurs in which swelling of the material completely closes the wicking channels, preventing further wicking and limiting liquid transport by a diffusion process (Akinli-Kogak, 2001).

When a textile structure is mechanically repeatedly requested, it may fail due to the breakage of the yarns/filaments by internal abrasion. Abrasion is the physical destruction of fibers, yarns, and fabrics, resulting from the rubbing of a textile surface over another surface. In case of internal abrasion, also called yarn-on-yarn abrasion, there is the rubbing of one yarn surface with another yarn surface (McKenna et al., 2004; Özdil et al., 2012). PET yarns have revealed a significant higher abrasion resistance than PP yarns, once the average number of loading

cycles was about 15 times higher than in case of PP. Many parameters may influence the abrasion resistance, namely the filament type, fineness, roughness, length, and mechanical properties. In general, polyester-based fibers present a higher abrasion resistance than PP based fibers (Özdil et al., 2012; Weller et al., 2013). Moreover, the use of finer filaments in the production of yarns increments the number of filaments in the cross-section, leading to a higher cohesion which results in better abrasion resistance as happens in case of PET yarns that have finer and more filaments than PP yarn (Özdil et al., 2012).

Once the produced braids are intended to be used as part of a more complex structure for partial tendons substitution, which requires a certain force, strain and stiffness level, the tensile mechanical properties of PP and PET yarns and braided structures were evaluated. From Fig. 7C and 7. C, it is possible to observe that as the number of yarns increases, for the same take-up rate, the load at failure also increases. This happens because there are more yarns available to withstand the applied load. Changing the take-up rate does not influence the load at failure once the number of yarns is the same (8 YH and 8 YL). However, the tenacity level, which is a usual measure of the specific stress at break in textile structures, is higher in case of 8 YH, once the two structures present a very similar load at failure but the 8 YH presents a lower tex value (Omeroglu, 2006; Hearle and Morton, 2008).

Regarding the strain to failure, it also increases as the number of yarns increases. This phenomenon may be explained by the increase of the braid angle with yarns number, which makes the yarns in structure take more time to align with the braid longitudinal axis and consequently with tensile load direction. For the same reason, when comparing the 8 YH and the 8 YL, the strain to failure increases when the take-up rate decreases due to the increase in braid angle (Omeroglu, 2006; Rawal et al., 2015). Therefore, the structure's stiffness, for both materials using a specific take-up rate, increases as the yarns number increases due to the force and strain levels relation. When the take-up rate decreases, for the same number of yarns, the stiffness decreases due to the strain level increase. Moreover, comparing the two 16 YH structures, the stiffness is higher when using the PET yarn, which is explained by the higher force and lower strain than when using the PP yarn. This is in accordance with the tensile properties when comparing the isolated yarns, being the PET yarn the one that presents the higher stiffness (Hearle and Morton, 2008). Besides that, the higher strain of PP_16 YH braid is also related with the higher braid angle than in case of PET_16 YH, what may be explained by the higher diameter of PP yarn (989.0 ± 1.7 μm) comparing to PET yarn (830.8 ± 1.6 μm). After evaluation of the braids tensile properties, the PET 16 YH structure was the selected one for further mechanical characterization once it presents the higher stiffness level, which is a demanding requirement for tendons substitution. Moreover, it has been reported a higher fatigue resistance when using multifilament PET yarns than PP yarns in ropes for marine energy devices, mostly due to the higher abrasion resistance (Weller et al., 2013).

The viscoelastic tendons behavior, means a time-dependent mechanical behavior, due to the viscous properties of the collagen fibers and ground substance, exhibiting creep, force-relaxation and mechanical hysteresis (energy dissipation). The relation between tendons force and strain is not constant, it depends on load level and time of displacement (Peltonen et al., 2010; James et al., 2008). Therefore, considering this viscoelastic behavior of tendons, it is also crucial to understand how the PET structures mechanical behavior is time-dependent.

Creep phenomenon is characterized by an increasing deformation under constant load, typically comprising three stages: a) primary stage occurring in the initial stage of loading when the creep rate decreases rapidly with time; b) secondary stage when creep rate reaches a steady-state; c) tertiary stage characterized by a rapid creep rate increase leading to creep failure. This contrasts with an elastic material, which does not exhibit increase of deformation no matter how long the load is applied. Creep deformations, which occur at lower forces, are recoverable after the load has been removed, given enough time. The major effect at low forces is a progressive straightening of molecules, often with a change in the links between molecular segments; this is usually recoverable and does not affect strength (Balani et al., 2015; Lechat et al., 2011; V-, Design, testing a). Creep deformations, at higher forces, are not totally recoverable. At those high forces, whole molecules slide past one another and this lead, eventually, to rupture. In general, during creep phenomenon, both recoverable and permanent deformations occur simultaneously. In force-relaxation phenomenon, the force withstand by the structure will decrease at a constant strain level. The stress required to maintain the constant strain value is decreased with time, because the molecules of polymer get relaxed with time, and to maintain the level of strain, somewhat lower value of stress is sufficient (Hearle and Morton, 2008; Balani et al., 2015; V-, Design, testing a).

The PET_16 YH braid revealed a very good resistance to creep, once its deformation remains almost the same over time, meaning a very low creep rate (creep curve slope) for all force levels (for instance, about 0.4 ± 0.2% for the 70% level) as observed in Fig. 8A, being more evident in Fig. 8B. The observed recoverable strain (ε_r), which is due to the elastic recoverable deformation of yarns but mainly of the structure by itself, tends to increase when the load level increases (Table 2) as already expected once the ε_{max} also increases (Hearle and Morton, 2008; V-, Design, testing a). The permanent strain, which is due to some plastic deformation of polymeric yarns, is very low and similar for all load levels, even at 70% of the load at failure. This is a very positive creep behavior attending to the final application of the structure, in which it will be exposed to different forces over long time periods. *Hawkins* et al., for instance, reported a strain increase of about 3.5% after 7 min of AT stimulation, which is really above the creep rate observed for these structures (Hawkins et al., 2009). Furthermore, the PET_16 YH structure revealed a low and similar relaxation rate for all strain levels as presented in Fig. 9C and more evident in Fig. 9D, meaning that when it is extended until different lengths it will be able to withstand the consequent load over long time periods without getting relaxed.

Attending the final application, the developed structures will be under long-term and repeated loading and they must remain working for a long time period. Thus, the fatigue resistance, which is one of the major reasons for failure in structural materials, of PET_16 YH structure was evaluated by exposure to different cyclic force levels. As observed in Fig. 10, the structure lifetime tends to decrease when the force level increases, as also reported for most materials. However, it must be noticed that for the level of 30% of the load at failure the structure was able to withstand 1 million cycles even at frequency of 5 Hz, which is really above the physiological frequency of 1.37 Hz (De Zee et al., 2000). The measured average daily walking activity reaches 1 to 2 million cycles per year (Silva et al., 2002). These fatigue tests assess the rope structure to sustain dynamic loads for at least 1.000.000 cycles at 1,37 Hz (equivalent to run during a year). However, the need to reduce 4 times the total tests duration led us to a higher frequency of 5 Hz. Clearly, higher frequencies produce within the fibrous structure, higher friction/abrasion, heat dissipation and, eventually, premature failure. Above all, the frequency of 5 Hz is more damaging than the physiological frequency of 1.37 Hz. Therefore, fatigue tests at 1.37 Hz, should produce a shift on the S–N curve to the right, therefore extending the number of cycles to failure.

This creep, relaxation and fatigue behavior of PET structure was already expected once that PET fibers are reported as being very interesting for different technical applications with demanding mechanical requirements and repeated use for long time periods (Lechat et al., 2011).

5. Conclusions

After the promoted characterization of all produced braids, it is possible to conclude that the braids architecture actually define their

physical and mechanical behavior, besides of course the intrinsic physical properties of the yarns that compose them. The number of yarns in the structure and the braiding take-up rate are the main parameters that can be adjusted to construct structures with different architectures, namely with a different braids/cm, diameter, linear density, tenacity, braid angle and porosity level. The wicking ability of braids was dependent on structure pores amount but also on how those pores communicate, which also depends on the architecture, namely how the yarns are arranged and packed in the structure.

The load failure level of the braids is mainly controlled by the number of yarns, but the strain level is mostly influenced by the take-up rate and consequently by the braid angle. Regarding the stiffness level, it results from a combination of the yarns number and braid angle. The PET_16 YH structure revealed a very promising creep and force-relaxation behavior for the final application, as well as a very interesting fatigue resistance. Therefore, PET_16 YH braids may be interesting structures to be used as elementary parts of a more complex textile structure in order to reach the real level of load at failure, strain to failure and stiffness of different tendons.

Author agreement

All authors of the paper titled: "Characterization of polypropylene (PP) and poly (ethylene terephthalate) (PET) multifilament braided textile structures for Achilles tendon partial substitution" agreed to the following points:

- The paper is not concurrently submitted for publication elsewhere
- The paper, in its entirety, in part, or in a modifies version, has not been published elsewhere
- The paper has not previously been submitted for possible publication elsewhere

Declaration of competing interest

The authors declare that they have no known competing financial interests or personal relationships that could have appeared to influence the work reported in this paper.

Acknowledgments

Authors acknowledge the financial support from FCT (Fundação para a Ciência e a Tecnologia), through the Grant SFRH/BD/88829/2012, Project PEst-C/EME/UI0285/2011 and Project UIDB/50006/2020.

References

Adanur, S., 1995. Wellington Sears Handbook of Industrial Textiles. CRC.
Akinli-Kogak, S., 2001. The Influence of Fiber Swelling on Paper Wetting. Citeseer.
Alagirusamy, R., Das, A., 2010. Technical Textile Yarns. Elsevier.
K. Balani, V. Verma, A. Agarwal, R. Narayan, Biosurfaces: A Materials Science and Engineering Perspective, John Wiley & Sons2015.
Bažant, Z.P., 1999. Size effect on structural strength: a review. Arch. Appl. Mech. 69 (9–10), 703–725.
Benltoufa, S., Fayala, F., Nasrallah, S.B., 2012. Determination of yarn and fiber diameters after swelling using a capillary rise method. J. Textil. Inst. 103 (5), 517–522.
Bicking, A.M., Oxenham, W., 2012. Variables and methods for aesthetic braid design. Journal of Textile and Apparel, Technology and Management 7 (4).
Calejo, I., Costa-Almeida, R., Reis, R.L., Gomes, M.E., 2019. A textile platform using continuous aligned and textured composite microfibers to engineer tendon-to-bone interface gradient scaffolds. Adv Healthc Mater 8 (15).
Chen, J., Xu, J., Wang, A., Zheng, M., 2009. Scaffolds for tendon and ligament repair: review of the efficacy of commercial products. Expet Rev. Med. Dev. 6 (1), 61–73.
Cooper, J.A., Lu, H.H., Ko, F.K., Freeman, J.W., Laurencin, C.T., 2005. Fiber-based tissue-engineered scaffold for ligament replacement: design considerations and in vitro evaluation. Biomaterials 26 (13), 1523–1532.
Cordage Institute International, August, 2001. Standard, Test Method for Yarn-On-Yarn Abrasion. CI 1503-00.
De, S.K., Aluru, N., Johnson, B., Crone, W., Beebe, D.J., Moore, J., 2002. Equilibrium swelling and kinetics of pH-responsive hydrogels: models, experiments, and simulations. Journal of Microelectromechanical Systems 11 (5), 544–555.
De Zee, M., Bojsen-Møller, F., Voigt, M., 2000. Dynamic viscoelastic behavior of lower extremity tendons during simulated running. J. Appl. Physiol. 89 (4), 1352–1359.
Fangueiro, R., Filgueiras, A., Soutinho, F., Meidi, X., 2010. Wicking behavior and drying capability of functional knitted fabrics. Textil. Res. J. 80 (15), 1522–1530.
Favaro, M.M., Branciforti, M.C., Bretas, R.E.S., 2009. A X-ray study of β-phase and molecular orientation in nucleated and non-nucleated injection molded polypropylene resins. Mater. Res. 12 (4), 455–464.
Hawkins, D., Lum, C., Gaydos, D., Dunning, R., 2009. Dynamic creep and pre-conditioning of the Achilles tendon in-vivo. J. Biomech. 42 (16), 2813–2817.
Hearle, J.W., Morton, W.E., 2008. Physical Properties of Textile Fibres. Elsevier.
Hess, G.W., 2010. Achilles tendon rupture: a review of etiology, population, anatomy, risk factors, and injury prevention. Foot Ankle Spec. 3 (1), 29–32.
Huang, Z., Bi, L., Zhang, Z., Han, Y., 2012. Effects of dimethylolpropionic acid modification on the characteristics of polyethylene terephthalate fibers. Mol. Med. Rep. 6 (4), 709–715.
Intziegianni, K., Cassel, M., Fröhlich, K., Engel, T., Mayer, F., 2015. Measuring achilles tendon length: a simple and reliable method. Sports Orthopaedics and Traumatology Sport-Orthopädie - Sport-Traumatologie 31 (4), 260–266.
James, R., Kesturu, G., Balian, G., Chhabra, A.B., 2008. Tendon: biology, biomechanics, repair, growth factors, and evolving treatment options. J. Hand Surg. 33 (1), 102–112.
Karathanasopoulos, N., Arampatzis, G., Ganghoffer, J.F., 2019. Unravelling the viscoelastic, buffer-like mechanical behavior of tendons: a numerical quantitative study at the fibril-fiber scale. J Mech Behav Biomed 90, 256–263.
Kuo, C.K., Marturano, J.E., Tuan, R.S., 2010. Novel strategies in tendon and ligament tissue engineering: advanced biomaterials and regeneration motifs, Sports medicine, arthroscopy, rehabilitation, therapy & technology. SMARTT 2, 20.
Kyosev, Y., 2014. Braiding Technology for Textiles: Principles, Design and Processes. Elsevier.
Laurencin, C.T., Freeman, J.W., 2005. Ligament tissue engineering: an evolutionary materials science approach. Biomaterials 26 (36), 7530–7536.
Lechat, C., Bunsell, A.R., Davies, P., 2011. Tensile and creep behaviour of polyethylene terephthalate and polyethylene naphthalate fibres. J. Mater. Sci. 46 (2), 528–533.
Lichtwark, G.A., Cresswell, A.G., Newsham-West, R.J., 2013. Effects of running on human Achilles tendon length-tension properties in the free and gastrocnemius components. J. Exp. Biol. 216 (23), 4388–4394.
Lim, W.L., Liau, L.L., Ng, M.H., Chowdhury, S.R., Law, J.X., 2019. Current progress in tendon and ligament tissue engineering. Tissue Eng Regen Med 16 (6), 549–571.
Longo, U.G., Lamberti, A., Maffulli, N., Denaro, V., 2010. Tendon augmentation grafts: a systematic review. Br. Med. Bull. 94, 165–188.
Maffulli, N., Renstrom, P., Leadbetter, W., 2005. Tendon Injuries-Basic Science and Clinical Medicine. Springer.
Martin, R.B., Burr, D.B., Sharkey, N.A., 1998. Mechanical Properties of Ligament and Tendon, Skeletal Tissue Mechanics. Springer New York, New York, NY, pp. 309–348.
H.A. McKenna, J.W. Hearle, N. O'Hear, Handbook of Fibre Rope Technology, Elsevier2004.
Modjarrad, K., Ebnesajjad, S., 2013. Handbook of Polymer Applications in Medicine and Medical Devices. Elsevier.
Morais, D., Rodrigues, M., Silva, T., Lopes, M., Santos, M., Santos, J., Botelho, C., 2013. Development and characterization of novel alginate-based hydrogels as vehicles for bone substitutes. Carbohydr. Polym. 95 (1), 134–142.
Morais, D., Torres, J., Guedes, R., Lopes, M., 2015. Current approaches and future trends to promote tendon repair. Ann. Biomed. Eng. 1–11.
Nunes, R.A.X., Costa, V.C., Calado, V.M.d.A., Branco, J.R.T., 2009. Wear, friction, and microhardness of a thermal sprayed PET: poly (ethylene terephthalate) coating. Mater. Res. 12 (2), 121–125.
Oh, D.S., Kim, Y.J., Hong, M.-H., Han, M.-H., Kim, K., 2014. Effect of capillary action on bone regeneration in micro-channeled ceramic scaffolds. Ceram. Int. 40 (7), 9583–9589.
Omeroglu, S., 2006. The effect of braiding parameters on the mechanical properties of braided ropes. Fibres Text. East. Eur. 14 (4), 53.
Özdil, N., Kayseri, G.Ö., Mengüç, G.S., 2012. Analysis of Abrasion Characteristics in Textiles. Marcin Adamiak, p. 119.
Peltonen, J., Cronin, N.J., Avela, J., Finni, T., 2010. In vivo mechanical response of human Achilles tendon to a single bout of hopping exercise. J. Exp. Biol. 213 (8), 1259–1265.
Potic, M., Ignjatovic, I., Savic, V., Djekic, P., Radenkovic, G., 2011. Mechanical properties and tissue reinforcement of polypropylene grafts used for pelvic floor repair—an experimental study. Hernia 15 (6), 685–690.
B.D. Ratner, A.S. Hoffman, F.J. Schoen, J.E. Lemons, Biomaterials Science: an Introduction to Materials in Medicine, Academic press2004.
Rawal, A., Saraswat, H., Sibal, A., 2015. Tensile response of braided structures: a review. Textil. Res. J. 85 (19), 2083–2096.
Rodrigues, M.T., Reis, R.L., Gomes, M.E., 2013. Engineering tendon and ligament tissues: present developments towards successful clinical products. Journal of tissue engineering and regenerative medicine 7 (9), 673–686.
Santos, M.L., Rodrigues, M.T., Domingues, R.M.A., Reis, R.L., Gomes, M.E., 2017. Biomaterials as tendon and ligament substitutes: current developments. In: Oliveira, J.M., Reis, R.L. (Eds.), Regenerative Strategies for the Treatment of Knee Joint Disabilities. Springer International Publishing, Cham, pp. 349–371.
Sarasua, J., Lopez-Rodriguez, N., Zuza, E., Petisco, S., Castro, B., Del Olmo, M., Palomares, T., Alonso-Varona, A., 2011. Crystallinity assessment and in vitro cytotoxicity of polylactide scaffolds for biomedical applications. J. Mater. Sci. Mater. Med. 22 (11), 2513–2523.
Saxena, S., Ray, A.R., Kapil, A., Pavon-Djavid, G., Letourneur, D., Gupta, B., Meddahi-Pellé, A., 2011. Development of a new polypropylene-based suture: plasma grafting,

surface treatment, characterization, and biocompatibility studies. Macromol. Biosci. 11 (3), 373–382.
Schwartz, P., 2008. Structure and Mechanics of Textile Fibre Assemblies. Elsevier.
Sharma, P., Maffulli, N., 2006. Biology of tendon injury: healing, modeling and remodeling. J. Musculoskelet. Neuronal Interact. 6 (2), 181–190.
Silva, M., Shepherd, E.F., Jackson, W.O., Dorey, F.J., Schmalzried, T.P., 2002. Average patient walking activity approaches 2 million cycles per year: pedometers under-record walking activity. J. Arthroplasty 17 (6), 693–697.
Tabbaa, S., Burg, K.J., 2015. The effect of wicking fibres in tissue-engineered bone scaffolds. Journal of tissue engineering and regenerative medicine 9 (4), 469–472.
S. Tabbaa, A. Mlynarczyk, K.J. Burg, Improved Cellular Recruitment and Mass Transport for Large Bone Defect Regeneration.
Veleirinho, B., Coelho, D.S., Dias, P.F., Maraschin, M., Pinto, R., Cargnin-Ferreira, E., Peixoto, A., Souza, J.A., Ribeiro-do-Valle, R.M., Lopes-da-Silva, J.A., 2014. Foreign body reaction associated with PET and PET/chitosan electrospun nanofibrous abdominal meshes. PloS One 9 (4), e95293.
Vořechovský, M., Chudoba, R., 2006. Stochastic modeling of multi-filament yarns: II. Random properties over the length and size effect. Int. J. Solid Struct. 43 (3), 435–458.
Weller, S., Davies, P., Johanning, L., Banfield, S., 2013. Guidance on the Use of Synthetic Fibre Ropes for Marine Energy Devices.
Wren, T.A.L., Yerby, S.A., Beaupre, G.S., Carter, D.R., 2001. Mechanical properties of the human Achilles tendon. Clin. Biomech. 16 (3), 245–251.